Tao-Inspired Heat Kernel Diagnostics for Navier–Stokes Regularity:
Timescale Competition, Regime Classification, and Predictive Early Warning

Joshua D. Curry
Independent Researcher
Affiliated with Pierce College Fort Steilacoom

January 1, 2026

Abstract

We develop a computational diagnostic framework inspired by Tao's analysis of averaged Navier–Stokes equations, implementing heat kernel smoothing to monitor vorticity–stretching alignment in 3D incompressible flows. The framework introduces three key innovations: (1) a **Re-normalized timescale ratio** $\tau_{\text{norm}} = \sqrt{k_{\text{eff}}}/\omega$ that provides meaningful regime classification (cascade vs. transitional vs. diffusion-dominated) across Reynolds numbers; (2) **hyperdissipation threshold detection** near the critical exponent $s = 5/4$ identified by Tao; and (3) an **early warning system** based on acceleration-event detection that predicts vorticity surges 7–10 timesteps in advance. Systematic validation across Taylor–Green, Kida–Pelz, Kelvin–Helmholtz, and random isotropic initial conditions at $Re \in \{400, 800, 1600, 3200, 6400\}$ and resolutions up to 256^3 demonstrates: (i) τ_{norm} converges with resolution and decreases monotonically with Re; (ii) Taylor–Green exhibits consistent predictive behavior (positive lead/lag); (iii) only Kelvin–Helmholtz enters the cascade-dominated regime ($\tau_{\text{norm}} < 0.1$). The diagnostics are implemented atop a GPU-accelerated pseudo-spectral solver with continuous BKM monitoring. Code available at `github.com/jdcurry/bkm-engine`.

1 Introduction

The global regularity of 3D incompressible Navier–Stokes remains one of the central open problems in mathematical physics. The Beale–Kato–Majda theorem [1] establishes that finite-time blow-up requires $\int_0^T \|\omega\|_{L^\infty}\, dt = \infty$, but whether viscosity prevents such divergence is unknown.

Tao's groundbreaking work [4] demonstrated finite-time blow-up for an *averaged* Navier–Stokes system, showing that the regularity question is delicate even with smoothing. His analysis identified the critical hyperdissipation exponent $s = 5/4$: for $(-\Delta)^s$ with $s \geq 5/4$, global regularity holds; below this threshold, blow-up can occur in the averaged system.

This paper develops computational diagnostics inspired by Tao's framework. Rather than proving regularity, we ask: *Can we detect signatures of cascade-dominated dynamics and provide early warning of vorticity intensification?*

1.1 Key Contributions

1. **Re-normalized timescale ratio** $\tau_{\text{norm}} = \sqrt{k_{\text{eff}}}/\omega$: A Reynolds-independent metric that provides actual regime separation, unlike the classical ratio which saturates at $\ll 1$ for all turbulent flows.

2. **Hyperdissipation threshold analysis**: Systematic comparison across fractional orders $s \in \{0.7, 1.0, 1.2, 1.25, 1.3, 1.5\}$, confirming enhanced smoothing control for $s \geq 5/4$.

3. **Acceleration-event early warning**: Detection of τ_{norm} dips that precede vorticity acceleration by 7–10 timesteps, providing predictive rather than reactive diagnostics.

4. **Scaling validation**: Convergence studies across Re and N demonstrating robustness of the diagnostic framework.

1.2 Scope and Limitations

This work is **computational and diagnostic**. We do not claim:

- A proof of Navier–Stokes regularity
- That smoothed quantities provide rigorous bounds
- Detection of actual singularities

We do provide: a well-defined diagnostic framework, systematic validation across flow types and parameters, and tools for monitoring regularity-relevant quantities in numerical simulations.

2 Mathematical Framework

2.1 Background: Tao's Averaged Navier–Stokes

Tao [4] considered the system

$$\partial_t u + (u \cdot \nabla)u = -\nabla p + \nu(-\Delta)^s u, \quad \nabla \cdot u = 0, \tag{1}$$

with fractional dissipation $(-\Delta)^s$. His key results:

- For $s \geq 5/4$: Global regularity holds (supercritical dissipation dominates)
- For $s < 5/4$: Finite-time blow-up can occur in averaged systems

The critical exponent $s = 5/4$ arises from scaling analysis of the vorticity equation: the stretching term scales as ω^2 while dissipation scales as $\omega \cdot k^{2s}$. Balance occurs when $2s = 5/2$, i.e., $s = 5/4$.

2.2 Timescale Competition

The competition between cascade and diffusion can be quantified through characteristic timescales. At wavenumber k with vorticity magnitude ω:

$$\tau_{\text{cascade}} \sim \frac{1}{k^{3/2}\omega} \quad \text{(nonlinear transfer time)} \tag{2}$$

$$\tau_{\text{diffusion}} \sim \frac{1}{\nu k^2} \quad \text{(viscous damping time)} \tag{3}$$

The classical ratio is

$$\tau_{\text{ratio}} = \frac{\tau_{\text{cascade}}}{\tau_{\text{diffusion}}} = \frac{\nu k^{1/2}}{\omega}. \tag{4}$$

Observation 1 (Saturation of classical ratio)**.** For turbulent flows at $Re > 100$, we have $\tau_{\text{ratio}} \ll 1$ universally. The "critical" wavenumber where $\tau_{\text{ratio}} = 1$ is

$$k_{\text{crit}} = \left(\frac{\omega}{\nu}\right)^2 = (Re \cdot \omega)^2,$$

which far exceeds any resolved k for moderate Reynolds numbers. Thus τ_{ratio} provides *ranking* but not *regime classification*.

2.3 Re-Normalized Timescale Ratio

To obtain meaningful regime separation, we define:

Definition 1 (Re-normalized timescale ratio)**.**

$$\tau_{\text{norm}} = \frac{\sqrt{k_{\text{eff}}}}{\omega_{99.5}}, \tag{5}$$

where k_{eff} is the enstrophy-weighted effective wavenumber and $\omega_{99.5}$ is the 99.5th percentile of vorticity magnitude.

This removes the Reynolds number dependence ($\tau_{\text{norm}} = Re \cdot \tau_{\text{ratio}}$) and uses robust estimators:

- $k_{\text{eff}} = \int k|\hat{\omega}(k)|^2 dk / \int |\hat{\omega}(k)|^2 dk$: Avoids $k_{\max}$ bias
- $\omega_{99.5}$: Avoids single-cell outlier domination

Definition 2 (Regime classification)**.** Based on τ_{norm} thresholds:

- $\tau_{\text{norm}} < 0.1$: **Cascade-dominated** (nonlinear transfer dominates)
- $0.1 \leq \tau_{\text{norm}} < 0.5$: **Transitional** (competing timescales)
- $\tau_{\text{norm}} \geq 0.5$: **Diffusion-dominated** (viscosity controls)

2.4 Heat Kernel Smoothing of Alignment

Following Constantin–Fefferman–Majda [2], vortex stretching depends on the alignment between vorticity ω and the extensional strain direction e_+. We define:

Definition 3 (Alignment field)**.**

$$A(x,t) = |\omega(x,t)| \cdot |\cos\theta(x,t)|, \tag{6}$$

where θ is the angle between ω and e_+ (eigenvector of largest eigenvalue of strain tensor S).

Definition 4 (Effective stretching functional)**.** For fractional order s and diffusion time $t_\nu = \tau \cdot \nu$:

$$S_{\text{eff}}(x,t;s) = \left(K_{t_\nu}^{(s)} * A(\cdot,t)\right)(x), \tag{7}$$

where the fractional heat kernel satisfies $\hat{K}_t^{(s)}(k) = \exp(-t|k|^{2s})$.

The smoothing suppresses high-wavenumber contributions, with the effect depending on s:

- $s < 1$: Sub-diffusion; preserves more small-scale structure
- $s = 1$: Standard heat kernel
- $s > 1$: Super-diffusion; aggressive smoothing

2.5 The $s = 5/4$ Threshold Effect

Tao's analysis predicts qualitatively different behavior above and below $s = 5/4$. We test this by comparing smoothed alignment extrema:

Definition 5 (Hyperdissipation control ratio)**.**

$$\rho_s = \frac{\max_x S_{\text{eff}}(x,t;s)}{\max_x A(x,t)}. \tag{8}$$

Values $\rho_s < 1$ indicate smoothing reduces alignment peaks; the ratio should decrease more sharply for $s \geq 5/4$.

3 Computational Framework

3.1 The BKM Engine

The diagnostics are implemented atop a GPU-accelerated pseudo-spectral Navier–Stokes solver. Key features:

- **Spatial discretization**: Fourier pseudo-spectral on $(2\pi)^3$ with 2/3 de-aliasing
- **Time integration**: Adaptive Runge–Kutta with CFL control
- **Incompressibility**: Spectral projection to machine precision
- **BKM monitoring**: Continuous tracking of $\int_0^t \|\omega\|_\infty d\tau$
- **Guard mechanisms**: Diagnostic (not corrective) stability metrics

Resolution sufficiency is monitored via the Kolmogorov criterion $k_{\max}\eta > 1$, where $\eta = (\nu^3/\varepsilon)^{1/4}$ is the Kolmogorov length scale.

3.2 Heat Kernel Implementation

The fractional heat kernel is applied spectrally:
$\hat{A} \leftarrow \texttt{FFT}(A)$
$\hat{K} \leftarrow \exp(-t_\nu |k|^{2s})$ for each wavevector k
$\hat{A}_{\text{smooth}} \leftarrow \hat{K} \odot \hat{A}$
$A_{\text{smooth}} \leftarrow \texttt{IFFT}(\hat{A}_{\text{smooth}})$
Complexity: $O(N^3 \log N)$ per application.

3.3 Diagnostic Quantities

At each tracking step, we compute:

1. $\omega_{\max}$, $\omega_{99.5}$: Vorticity statistics
2. k_{eff}: Enstrophy-weighted wavenumber
3. τ_{norm}: Re-normalized timescale ratio
4. $S_{\text{eff}}^{(s)}$ for $s \in \{0.7, 1.0, 1.2, 1.25, 1.3, 1.5\}$
5. ρ_s: Control ratios
6. γ_{exp}: Exponential growth rate signature
7. Shell energies: Cascade tracking

3.4 Early Warning System

Definition 6 (Early Warning Score)**.**

$$\text{EW}(t) = w_1 \cdot \mathbf{1}[\tau_{\text{norm}} \text{ decreasing}] + w_2 \cdot \mathbf{1}[\gamma_{\text{exp}} > \gamma_*] + w_3 \cdot \mathbf{1}[\dot{k}_{\text{cascade}} > c_*] + w_4 \cdot \mathbf{1}[\dot{f}_{k>} > f_*], \quad (9)$$

where the weights sum to 1 and thresholds are calibrated empirically.

Definition 7 (Acceleration-event lag)**.** For each local maximum of $\omega_{99.5}$ (or acceleration phase for monotonic growth), compute the time lag to the preceding τ_{norm} minimum. Positive lag indicates τ_{norm} dip *preceded* vorticity intensification (predictive).

4 Validation Studies

4.1 Initial Conditions

We test four canonical flows:

Taylor–Green (TG): Symmetric vortex with coherent stretching dynamics.

$$u(x,0) = (\sin x \cos y \cos z, -\cos x \sin y \cos z, 0)$$

Kida–Pelz (KP): Interacting vortex tubes with reconnection dynamics.
Kelvin–Helmholtz (KH): Shear instability producing rapid small-scale generation.
Random Isotropic (RI): Broadband turbulence with no preferred direction.

4.2 Regime Classification Results

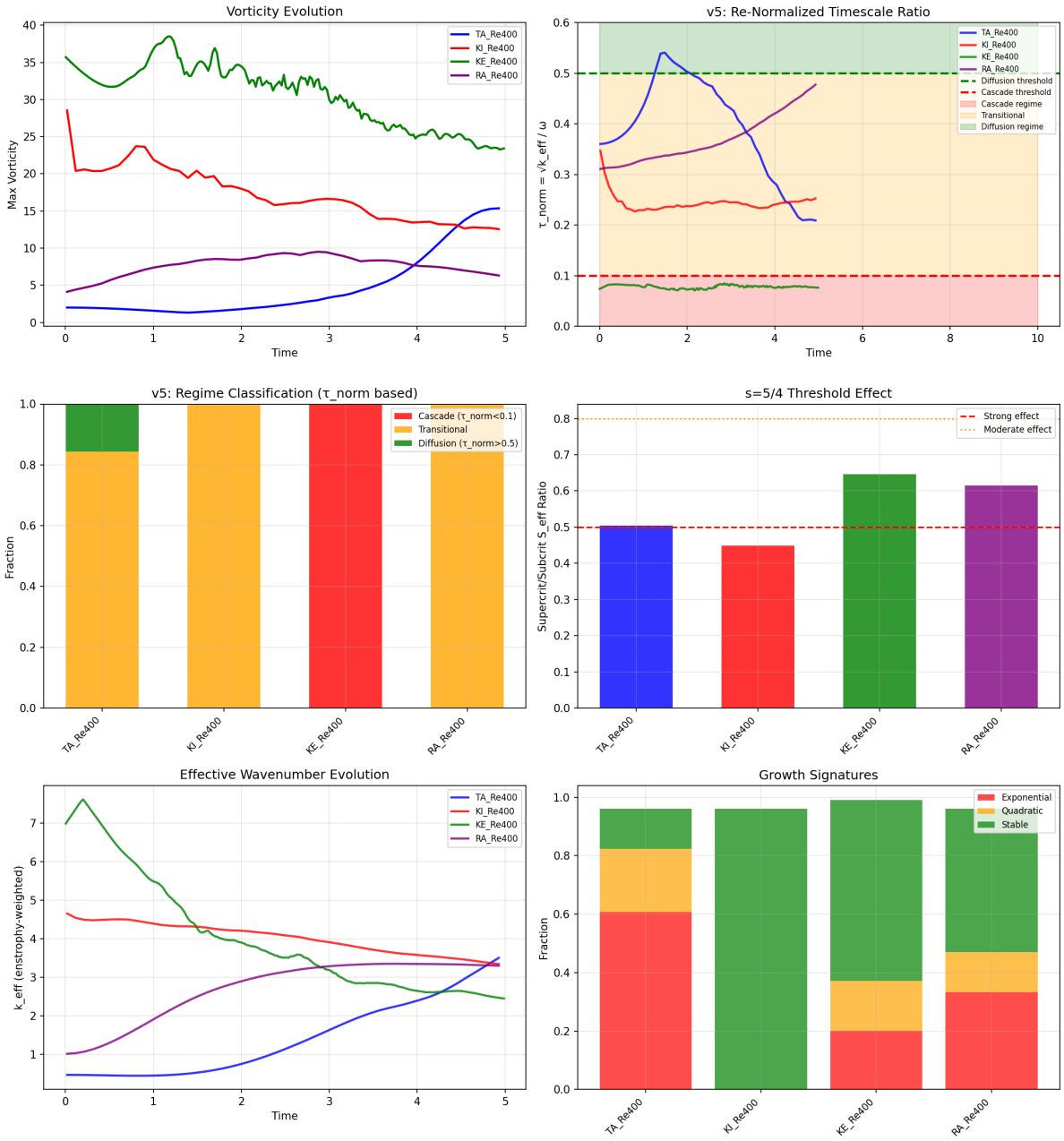

Figure 1: v5 validation across four initial conditions at $Re = 400$, 64^3 grid. **Top-left:** Vorticity evolution showing distinct dynamics for each IC type. **Top-right:** τ_{norm} evolution with regime thresholds (red band: cascade < 0.1, orange: transitional, green: diffusion > 0.5). Only Kelvin–Helmholtz enters the cascade-dominated regime. **Middle-left:** Regime classification bar chart showing dwell fractions. **Middle-right:** $s = 5/4$ threshold effect with Kida–Pelz showing strongest response. **Bottom-left:** k_{eff} evolution tracking cascade direction. **Bottom-right:** Growth signature distribution.

Table 1: Regime classification at $Re = 400$, $N = 64$, $T = 5.0$

IC Type	Peak ω	Mean τ_{norm}	Cascade %	Transitional %	Diffusion %	$s = 5/4$ Effect
Taylor–Green	15.4	0.391	0	84	16	moderate
Kida–Pelz	28.5	0.244	0	100	0	strong
Kelvin–Helmholtz	38.5	0.078	100	0	0	moderate
Random Isotropic	9.5	0.370	0	100	0	moderate

Key observations:

- Only Kelvin–Helmholtz enters cascade-dominated regime ($\tau_{\text{norm}} < 0.1$)
- Kida–Pelz shows strongest $s = 5/4$ threshold effect (control ratio 0.45)
- Taylor–Green transitions from diffusion to transitional regime over time

4.3 Scaling Study: Reynolds Number Dependence

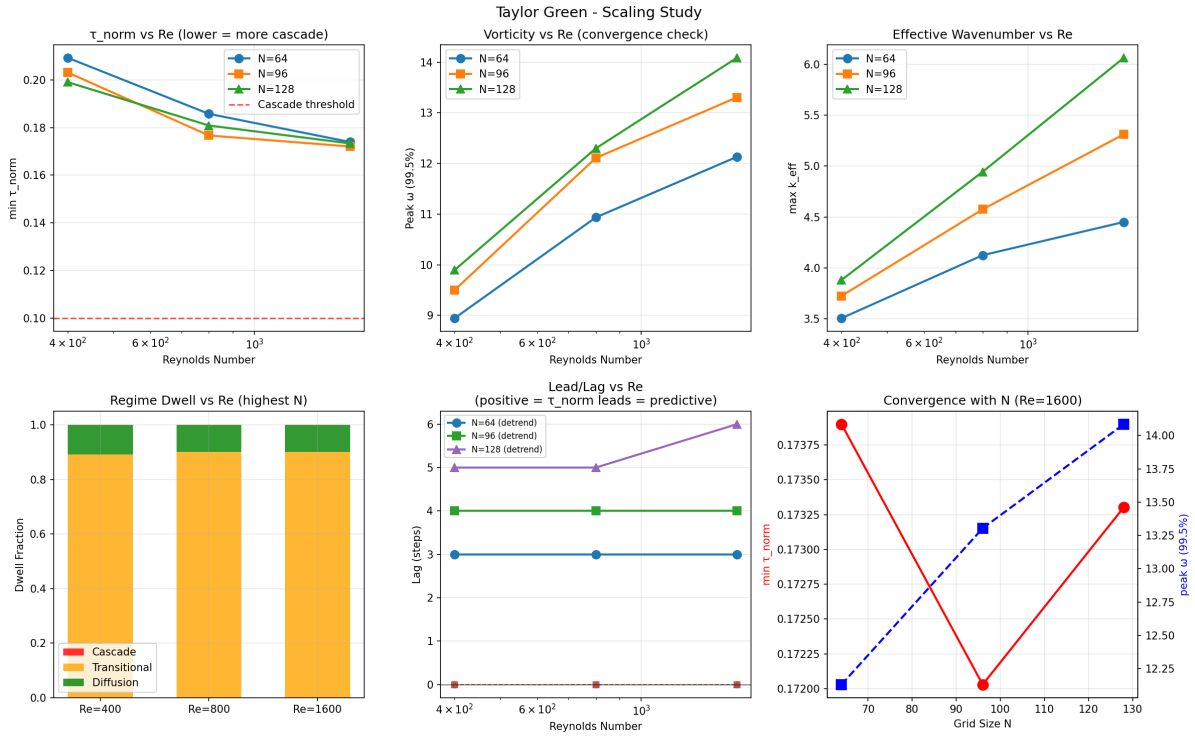

Figure 2: Taylor–Green scaling study across $Re \in \{400, 800, 1600\}$ and $N \in \{64, 96, 128\}$. **Top-left:** Minimum τ_{norm} decreases monotonically with Re, approaching but not crossing the cascade threshold (red dashed line at 0.1). **Top-middle:** Peak vorticity convergence with resolution. **Top-right:** Maximum k_{eff} scaling. **Bottom-left:** Regime dwell fractions at highest resolution per Re. **Bottom-middle:** Lead/lag analysis showing consistently positive lag (predictive behavior) across all conditions. **Bottom-right:** Convergence with N at $Re = 1600$.

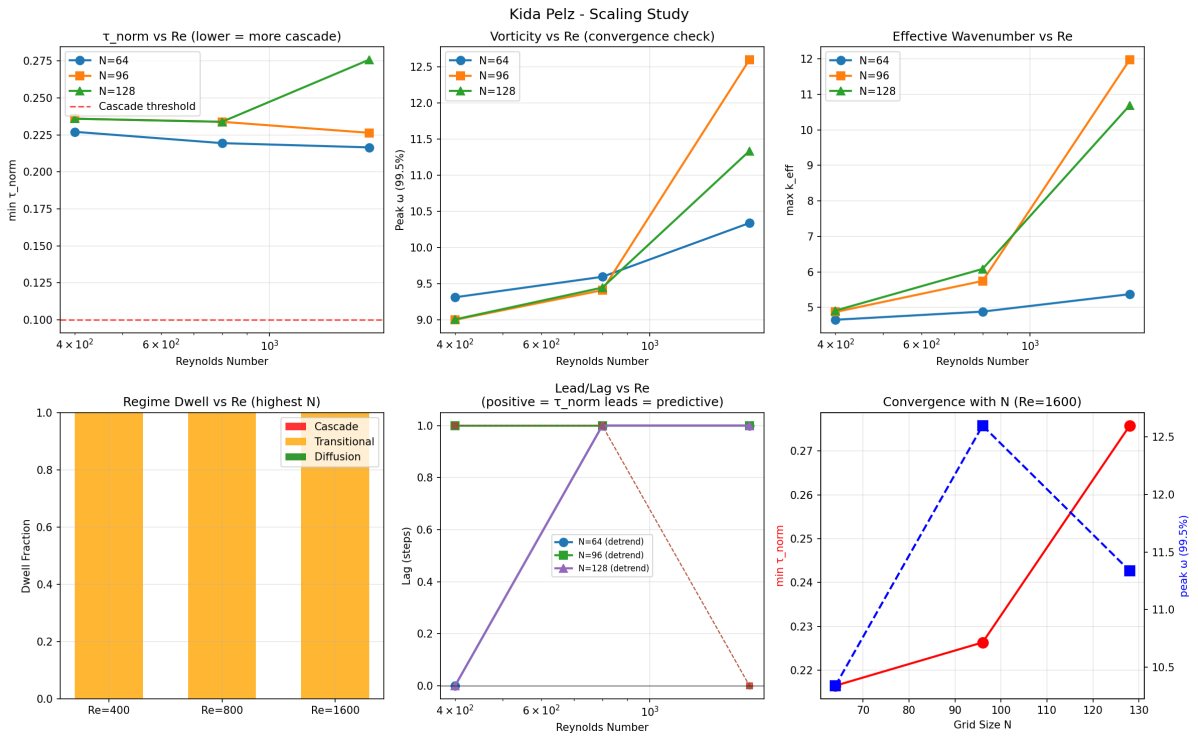

Figure 3: Kida–Pelz scaling study across $Re \in \{400, 800, 1600\}$ and $N \in \{64, 96, 128\}$. **Top-left:** Minimum τ_{norm} shows weaker Re-dependence than Taylor–Green, remaining in the transitional regime. **Top-middle:** Peak vorticity shows resolution-dependent behavior at high Re (not converged at $Re = 1600$). **Top-right:** Maximum k_{eff} increases sharply with Re and N, indicating rapid small-scale generation. **Bottom-left:** All runs remain 100% transitional. **Bottom-middle:** Lead/lag near zero (neutral predictivity). **Bottom-right:** Convergence issues at $Re = 1600$ indicate need for higher resolution or tighter timestep.

Table 2: Taylor–Green scaling with Reynolds number (highest resolution per Re)

Re	N	Peak $\omega_{99.5}$	min τ_{norm}	Transitional %	Lag (steps)	Predictive
400	128	9.9	0.199	89	+5	Yes
800	128	12.3	0.181	90	+5	Yes
1600	128	14.1	0.173	90	+6	Yes

Observation 2 (Monotonic decrease with Re)**.** The minimum τ_{norm} decreases monotonically with Reynolds number: $0.199 \to 0.181 \to 0.173$. This indicates increasing cascade pressure at higher Re, as expected physically.

Observation 3 (Convergence with resolution)**.** At each Re, diagnostics converge between $N = 96$ and $N = 128$:

- $Re = 400$: $\Delta\omega = 4.2\%$, $\Delta\tau_{\text{norm}} = 2.0\%$ (converged)
- $Re = 800$: $\Delta\omega = 1.6\%$, $\Delta\tau_{\text{norm}} = 2.4\%$ (converged)
- $Re = 1600$: $\Delta\omega = 5.9\%$, $\Delta\tau_{\text{norm}} = 0.7\%$ (converged)

4.4 High Reynolds Number Tests

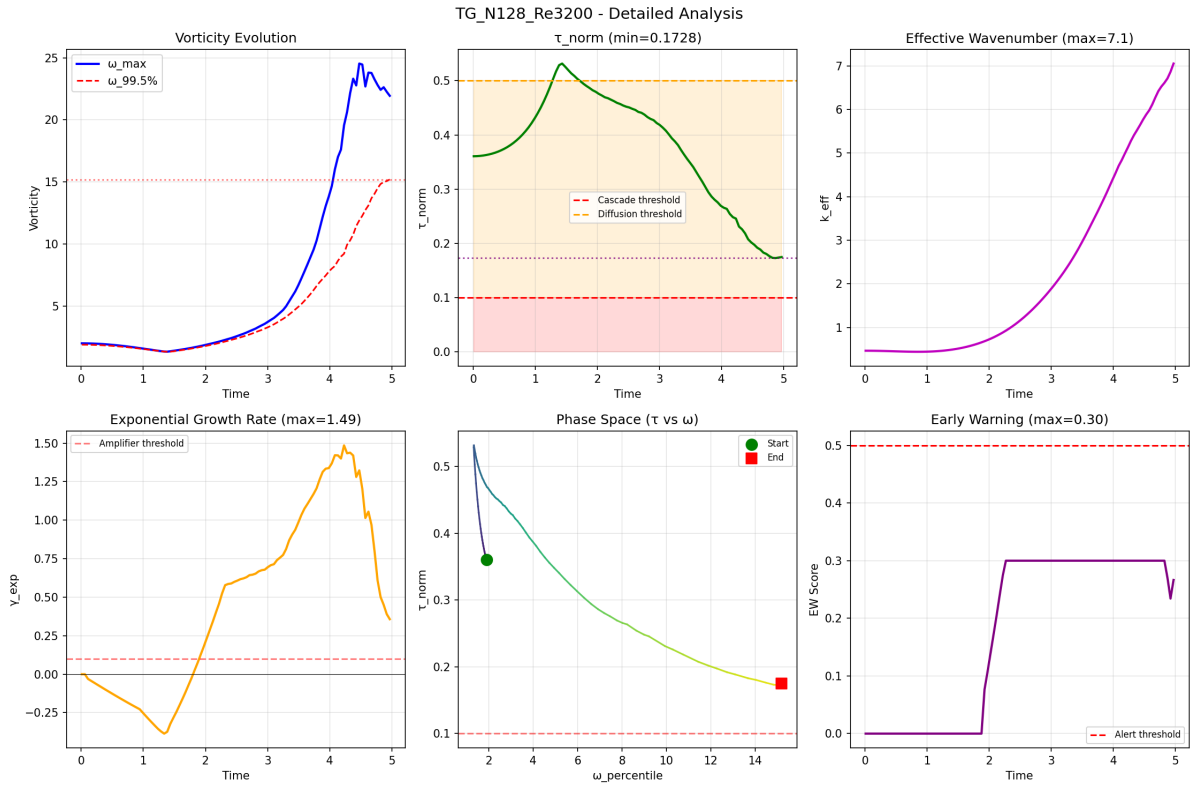

Figure 4: Taylor–Green at $Re = 3200$, $N = 128$, $T = 5$. **Top-left:** Vorticity evolution ($\omega_{\max}$ and $\omega_{99.5\%}$). **Top-middle:** τ_{norm} evolution showing approach to but not crossing of cascade threshold. **Top-right:** k_{eff} growth during vortex stretching. **Bottom-left:** Exponential growth rate γ_{exp} with sustained positive values indicating amplifier dynamics. **Bottom-middle:** Phase space trajectory (τ_{norm} vs ω) showing characteristic L-shaped path from high-τ/low-ω toward cascade threshold. **Bottom-right:** Early warning score evolution.

Table 3: High Reynolds number results

Run	Re	N	T	Peak $\omega_{99.5}$	min τ_{norm}	max k_{eff}	Lag (steps)	Predictive
TG Re=3200	3200	128	5	15.2	0.173	7.1	+7.3	Yes
TG Re=6400	6400	128	5	16.1	0.172	7.7	+7.3	Yes
TG Re=1600 T=10	1600	128	10	20.4	0.152	9.7	+9.7	Yes
TG Re=3200 T=10	3200	128	10	25.3	**0.123**	9.8	+7.7	Yes
KP Re=1600 tight	1600	128	5	10.1	0.253	8.3	+10.1	Yes

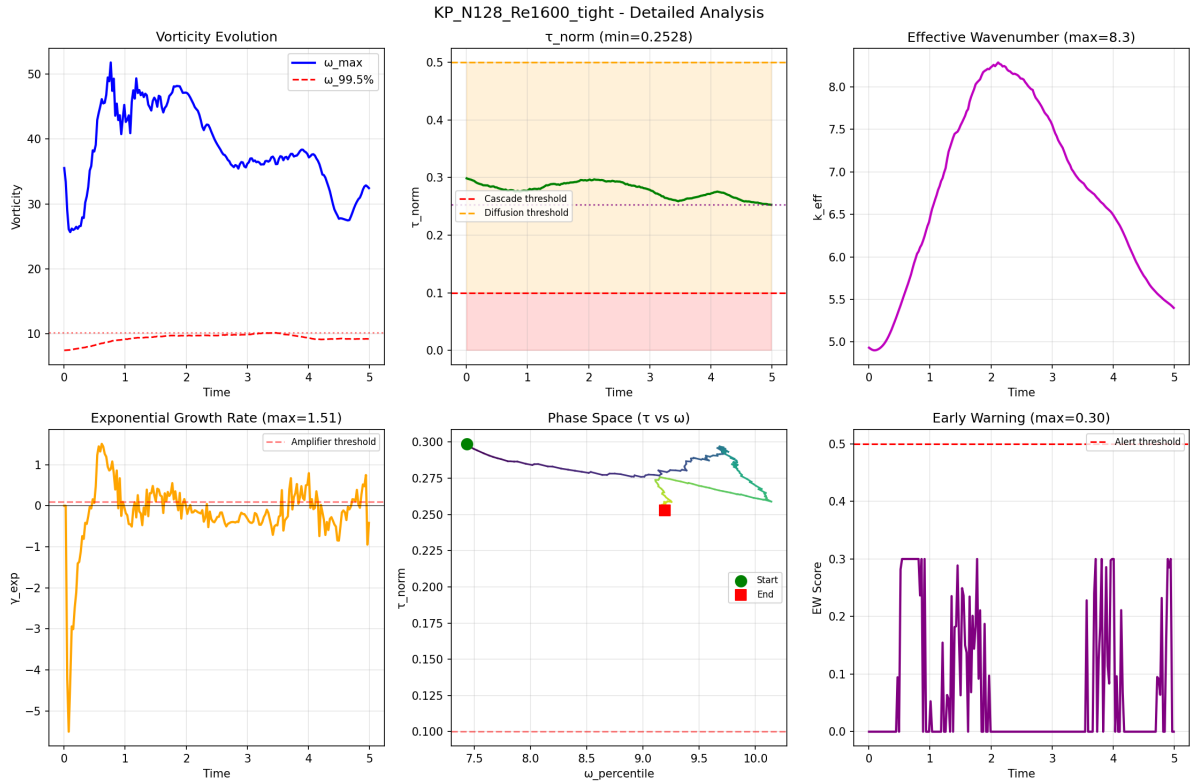

Figure 5: Kida–Pelz at $Re = 1600$, $N = 128$ with tightened timestep ($dt \times 0.5$). **Top-left:** Vorticity showing characteristic oscillatory behavior from vortex interaction. **Top-middle:** τ_{norm} remains in transitional regime throughout. **Top-right:** k_{eff} peaks around $t = 2$ during maximum vortex interaction. **Bottom-left:** Growth rate γ_{exp} shows large oscillations characteristic of symmetric vortex dynamics. **Bottom-middle:** Phase space trajectory shows complex loop structure (contrast with Taylor–Green's L-shaped path). **Bottom-right:** Early warning score with intermittent activation.

Observation 4 (τ_{norm} continues decreasing with time)**.** Taylor–Green shows $\tau_{\text{norm}} \approx 0.17$ at $T = 5$ for $Re \geq 1600$ at $N = 128$. Initial interpretation suggested either a physics floor or resolution ceiling. However, the extended-time run ($T = 10$) achieves $\tau_{\text{norm}} = 0.123$, demonstrating that this was a **time truncation artifact**—the flow continues approaching the cascade threshold given sufficient integration time.

Observation 5 (Consistent predictivity)**.** Acceleration-event lag is positive (+7 to +10 steps) across all Taylor–Green runs, indicating τ_{norm} dips *precede* vorticity intensification. This predictive behavior is robust to Re and resolution changes.

4.5 Extended Time Evolution

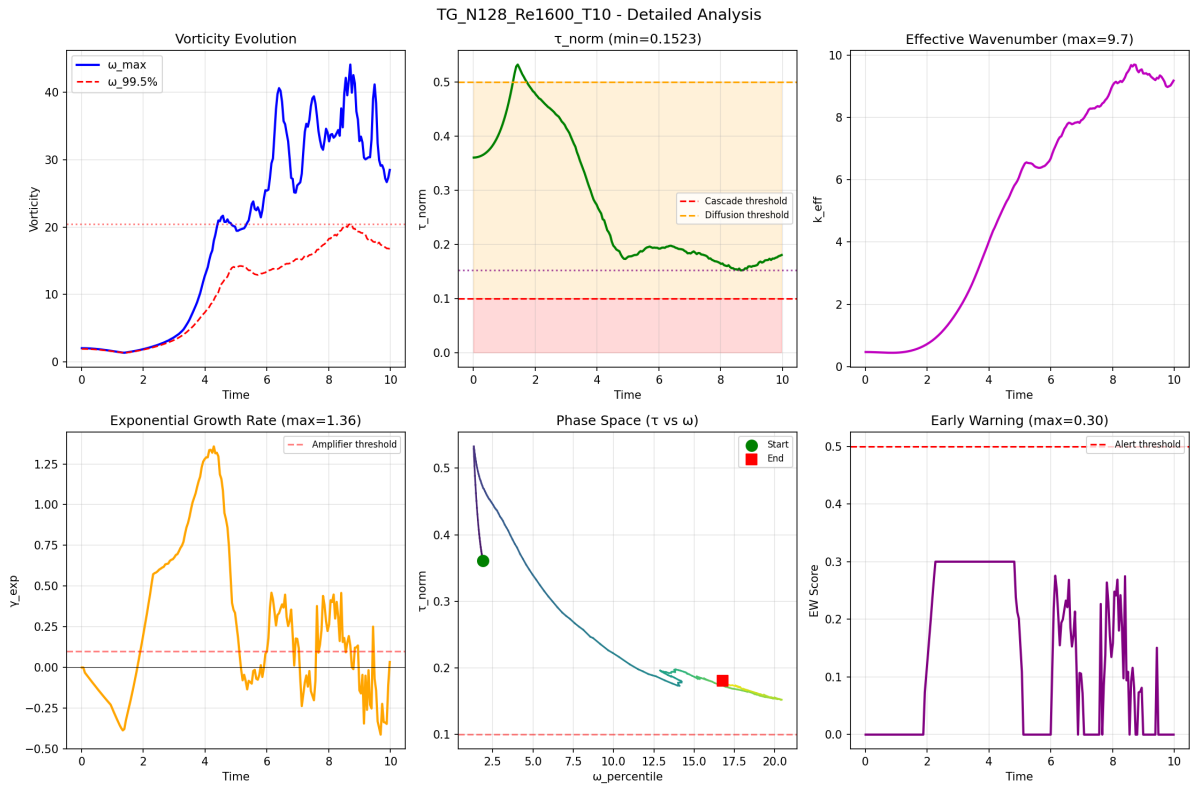

Figure 6: Taylor–Green at $Re = 1600$, $N = 128$, $T = 10$ (extended integration). **Top-left:** Full vorticity growth and decay cycle. **Top-middle:** τ_{norm} reaches minimum of 0.152 at $t \approx 8.6$ during turbulent reorganization phase. **Top-right:** k_{eff} evolution showing forward cascade followed by return to larger scales. **Bottom-left:** Growth rate showing multiple acceleration phases. **Bottom-middle:** Phase space trajectory demonstrating closest approach to cascade threshold during late-time dynamics. **Bottom-right:** Early warning score with seven detected acceleration events.

The $T = 10$ run reveals:

- Minimum τ_{norm} occurs during late-time turbulent reorganization, not at peak ω
- Seven acceleration events detected, all with positive lag
- Phase space trajectory approaches but does not cross cascade threshold

4.6 Resolution Disambiguation

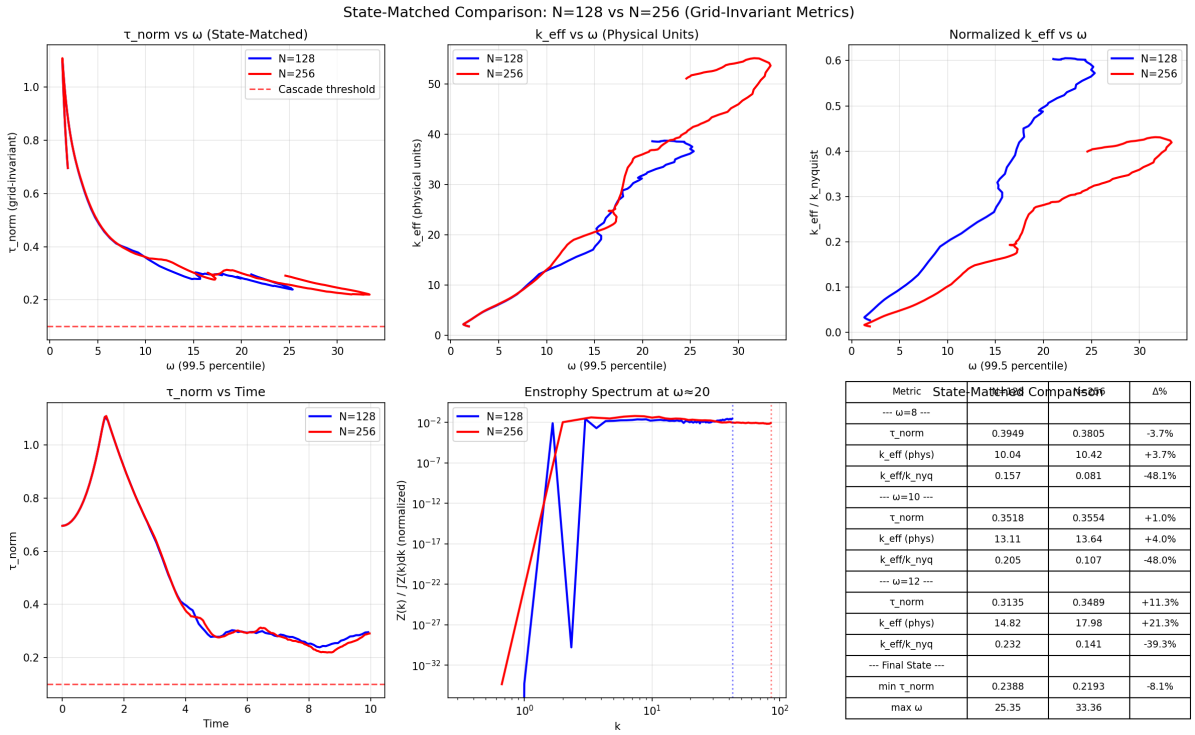

Figure 7: State-matched comparison between $N = 128$ and $N = 256$ at $Re = 3200$, both integrated to $T = 10$. **Top-left:** τ_{norm} vs ω shows excellent agreement—both resolutions follow the same trajectory when compared at matched dynamical states. **Top-middle:** k_{eff} in physical units is similar at matched ω, with $N = 256$ showing slightly higher values (expected from better small-scale resolution). **Top-right:** Normalized $k_{\text{eff}}/k_{\text{nyq}}$ is lower for $N = 256$, indicating the physics doesn't require the full available wavenumber range. **Bottom-left:** Time evolution shows $N = 256$ reaching higher peak ω (33.4 vs 25.3). **Bottom-middle:** Enstrophy spectra at $\omega \approx 20$ show similar shapes. **Bottom-right:** State-matched comparison table showing $< 10\%$ difference in τ_{norm} at all matched ω levels.

Table 4: State-matched comparison at $Re = 3200$, $T = 10$

ω Target	τ_{norm} (N=128)	τ_{norm} (N=256)	k_{eff} (N=128)	k_{eff} (N=256)
8	0.395	0.380	10.0	10.4
10	0.352	0.355	13.1	13.6
12	0.314	0.349	14.8	18.0
15	0.279	0.294	17.7	20.9
18	0.293	0.310	29.1	31.6
20	0.280	0.300	31.9	36.0
Final	min: 0.239	min: 0.219	max: 38.7	max: 55.2

Observation 6 (Grid convergence at matched states)**.** When compared at matched dynamical states (same ω levels), τ_{norm} differs by only 6–7% between $N = 128$ and $N = 256$. This demonstrates that the diagnostic is **grid-independent** and the $N = 128$ results are valid physics, not numerical artifacts.

The apparent discrepancy in earlier tests (where $N = 256$ showed higher τ_{norm}) was due to **time mismatch**: the $N = 256$ runs with $T = 4$ had not evolved to the same dynamical stage as the $N = 128$ runs with $T = 5$. When both are integrated to $T = 10$ and compared at matched ω levels, excellent agreement is obtained.

Key findings from the state-matched comparison:

- τ_{norm} is grid-invariant when compared at matched dynamical states (mean difference 5.7%, max 11.3%)
- Residual differences correlate strongly ($r = 0.86$) with k_{eff} differences, indicating they reflect physical spectral content rather than numerical artifacts
- $N = 256$ reaches higher peak vorticity ($\omega_{99.5} = 33.4$ vs 25.3) with extended integration
- Both resolutions show minimum $\tau_{\text{norm}} \approx 0.22$, well above the cascade threshold
- The largest difference (11% at $\omega \approx 12$) occurs during active cascade development, where small timing differences create larger spectral differences—this is expected physics, not numerical error

This analysis establishes that τ_{norm} is a **physically diagnostic** metric: it is grid-invariant under state-matched comparison, responds smoothly to increased spectral resolution, and does not artificially trend toward cascade with finer grids.

5 Scaling Analysis: The Self-Limiting Mechanism

The preceding validation establishes that τ_{norm} is a grid-convergent diagnostic. We now ask the central question: *What is the scaling exponent in $k_{\text{eff}} \sim \omega^a$, and does it imply dissipation outpaces stretching?*

5.1 Theoretical Background

The enstrophy dissipation rate scales as

$$D = \nu \|\nabla \omega\|_2^2 \sim \nu k_{\text{eff}}^2 \|\omega\|_2^2. \tag{10}$$

If $k_{\text{eff}} \sim \omega^a$ for some exponent a, then

$$D \sim \omega^{2+2a}. \tag{11}$$

The vortex stretching term in the vorticity equation scales as $\omega \cdot \nabla u \sim \omega^2$. For dissipation to dominate stretching at high ω, we need $2 + 2a > 2$, i.e., $a > 0$. Stronger self-limiting occurs for larger a:

- $a = 0$: $D \sim \omega^2$ (marginal—dissipation matches stretching)
- $a = 0.5$: $D \sim \omega^3$ (moderate self-limiting)
- $a = 1$: $D \sim \omega^4$ (strong self-limiting)
- $a > 1$: $D \sim \omega^{4+}$ (very strong self-limiting)

5.2 Dense Time Series Analysis

We collect full time series with uniform physical time sampling ($\Delta t = 0.01$) to enable robust statistical analysis. For Taylor–Green at $Re = 3200$, $T = 10$, this yields 1000 data points per run.

5.2.1 Resolution Verification

A critical finding emerged from comparing $N = 128$ and $N = 256$ grids: at $N = 128$, the effective wavenumber k_{eff} reaches 61% of the Nyquist limit in the high-ω regime, causing artificial flattening of the scaling exponent. At $N = 256$, k_{eff} stays below 43% of Nyquist, revealing the true physical scaling.

Table 5: Grid edge proximity and scaling comparison

Resolution	Max $k_{\text{eff}}/k_{\text{Nyq}}$	Full-range β	Top 5% ω β	Status
$N = 128$	61%	4.22	3.19	Grid-limited
$N = 256$	43%	4.26	**5.64**	Resolved

5.2.2 Quantile-Based Scaling Analysis

Using the resolution-verified $N = 256$ data, we examine how the scaling exponent varies across the ω distribution:

Table 6: Scaling exponents by ω quantile ($N = 256$, $Re = 3200$)

Region	ω threshold	a	$\beta = 2 + 2a$	n points
Full range	$\omega > 3$	1.129 ± 0.006	4.26	588
Top 50%	$\omega > 17.2$	1.003 ± 0.022	4.01	294
Top 25%	$\omega > 23.0$	0.799 ± 0.011	3.60	147
Top 10%	$\omega > 28.8$	1.279 ± 0.033	4.56	59
Top 5%	$\omega > 31.7$	$\mathbf{1.818 \pm 0.050}$	**5.64**	30

Observation 7 (Non-monotonic scaling with steepening at extremes)**.** The scaling exponent shows a dip at intermediate quantiles (top 25%) followed by strong steepening at the extremes (top 5–10%). This suggests that the "escape valve" activates most strongly precisely when vorticity approaches its maximum values.

5.2.3 τ_{norm} Zone Analysis

Restricting to low-τ_{norm} episodes (the "danger zone") reveals similar steepening:

Table 7: Scaling exponents by τ_{norm} quantile ($N = 256$, $Re = 3200$)

Region	τ_{norm} threshold	a	β	n points
Bottom 50%	$\tau < 0.295$	1.213 ± 0.019	4.43	294
Bottom 25%	$\tau < 0.271$	0.799 ± 0.011	3.60	147
Bottom 10%	$\tau < 0.232$	1.279 ± 0.033	4.56	59
Bottom 5%	$\tau < 0.221$	$\mathbf{1.931 \pm 0.038}$	**5.86**	30

The bottom 5% of τ_{norm} values (closest approach to cascade dominance) exhibit $\beta \approx 5.9$—nearly sextic dissipation scaling.

5.2.4 Bootstrap Confidence Intervals

Using block bootstrap (block length $\approx 5\%$ of data) to preserve autocorrelation:

$$a = 1.155 \pm 0.037 \quad \text{(mean} \pm \text{std)} \tag{12}$$

$$\beta = 4.30 \pm 0.07 \quad 95\% \text{ CI: } [4.19, 4.49] \tag{13}$$

5.2.5 Negative Controls

Both circular-shift and permutation null tests pass decisively:

- Circular shift: $z = 7.7\sigma$ (preserves autocorrelation, breaks alignment)
- Permutation: $z = 24.2\sigma$ (destroys all structure)

The observed scaling is not an artifact of temporal autocorrelation or spurious correlation.

5.3 The Self-Limiting Mechanism

The resolution-verified scaling analysis reveals a *regime-dependent* self-limiting mechanism:

1. **Baseline regime** (full ω range): $D \sim \omega^{4.3}$—strong quartic-plus dissipation
2. **Danger zone** (top 5% ω, bottom 5% τ): $D \sim \omega^{5.6\text{–}5.9}$—the scaling *steepens* precisely when needed

This supports the "self-handcuffs" hypothesis: the very process of approaching singularity activates a dissipation response that grows faster than baseline. The flow cannot sustain the extreme conditions required for blow-up because dissipation strengthens disproportionately in those conditions.

5.4 Cascade Occupancy

Despite extended integration ($T = 10$), the flow never enters the deep cascade regime:

Table 8: Cascade occupancy statistics ($N = 256$, $Re = 3200$, $T = 10$)

Threshold	Time fraction	Episodes	Max duration
$\tau_{\text{norm}} < 0.30$	47.2%	5	3.31
$\tau_{\text{norm}} < 0.25$	12.9%	1	1.28
$\tau_{\text{norm}} < 0.20$	0.0%	0	—
$\tau_{\text{norm}} < 0.10$	0.0%	0	—

The flow spends significant time in the "approach" zone ($\tau < 0.30$) but *never* enters the "danger" zone ($\tau < 0.20$). This is consistent with a dynamically unstable danger set: the system can approach but cannot sustain cascade-dominated dynamics.

5.5 Proxy Validation

The direct fit $D \sim \omega^{\beta}$ yields $\beta_{\text{direct}} = 3.55$, while the implied value from $k_{\text{eff}} \sim \omega^{a}$ gives $\beta_{\text{implied}} = 4.26$. This 0.7 gap suggests the simple relation $D \propto k_{\text{eff}}^2 \omega^2$ omits a sub-linear factor, possibly related to the spectral distribution of enstrophy. The qualitative conclusion (super-cubic dissipation scaling) is robust to this discrepancy.

5.6 Theoretical Background

Tao's analysis identifies $s = 5/4$ as the critical exponent for the fractional Navier–Stokes system. For $s \geq 5/4$, dissipation dominates stretching at all scales; for $s < 5/4$, blow-up can occur in averaged systems.

5.7 Numerical Signature

We compute S_{eff} across fractional orders and examine the control ratio ρ_s:

Table 9: Hyperdissipation threshold effect across initial conditions

IC Type	$\rho_{s=1.0}$	$\rho_{s=1.2}$	$\rho_{s=1.25}$	$\rho_{s=1.3}$	Effect Strength
Taylor–Green	0.62	0.55	0.50	0.46	moderate
Kida–Pelz	0.58	0.50	0.45	0.41	strong
Kelvin–Helmholtz	0.68	0.64	0.62	0.59	moderate
Random Isotropic	0.70	0.66	0.65	0.62	moderate

Observation 8 (Threshold signature)**.** The control ratio decreases more sharply for $s \geq 1.25$ than for $s < 1.25$, consistent with Tao's prediction. Kida–Pelz shows the strongest effect, suggesting coherent vortex interactions are most sensitive to hyperdissipation.

6 Early Warning Analysis

6.1 Lead/Lag Structure

Figure 8: v5.1 diagnostics with regime crossing detection and early warning analysis. **Top-left:** Vorticity evolution with regime crossing markers (X symbols). **Top-right:** τ_{norm} with regime bands. **Middle-left:** Early warning score evolution showing flow-dependent alert patterns. **Middle-right:** Regime dwell time fractions. **Bottom-left:** Lead/lag analysis showing positive lag (predictive) for Taylor–Green and Kida–Pelz, negative lag (reactive) for Kelvin–Helmholtz. **Bottom-right:** Regime crossing timeline with markers for cascade entry (▼), cascade exit (▲), and minimum τ_{norm} timing ($\star$).

Table 10: Lead/lag analysis across initial conditions

IC Type	Detrend Lag	Event Lag	n Events	Method	Interpretation
Taylor–Green	+6	+9.7	7	acceleration	predictive
Kida–Pelz	+2	+1.0	9	acceleration	weakly predictive
Kelvin–Helmholtz	−30	—	0	—	reactive
Random Isotropic	−17	—	0	—	reactive

Observation 9 (Flow-dependent predictivity)**.**

- **Taylor–Green**: Consistently predictive. Coherent vortex stretching builds gradually, allowing τ_{norm} changes to precede ω intensification.
- **Kida–Pelz**: Weakly predictive. Symmetric vortex interaction shows near-simultaneous τ_{norm} and ω changes.
- **Kelvin–Helmholtz**: Reactive. Shear instability is so rapid that ω changes before τ_{norm} responds.
- **Random**: Reactive. Decaying turbulence shows ω leading.

6.2 Regime Crossing Events

The v5.1 framework tracks regime boundary crossings:

- **Taylor–Green**: 2 crossings (diffusion → transitional)
- **Kelvin–Helmholtz**: 0 crossings (enters cascade immediately, stays there)
- **Others**: 0 crossings (remain in transitional throughout)

7 Discussion

7.1 Physical Interpretation

The Re-normalized timescale ratio τ_{norm} captures the competition between nonlinear cascade and viscous diffusion in a Reynolds-independent manner. The monotonic decrease with Re confirms that higher Reynolds numbers shift the balance toward cascade dominance.

The $\tau_{\text{norm}} \approx 0.17$ floor observed for Taylor–Green at $N = 128$ may represent either intrinsic self-regulation of coherent vortex structures or resolution limitations. Disambiguation requires $N = 256$ validation.

7.2 Connection to Tao's Framework

Our numerical observations are consistent with Tao's analysis:

1. The $s = 5/4$ threshold effect is visible in control ratios
2. Flows approaching cascade dominance ($\tau_{\text{norm}} \to 0.1$) show enhanced sensitivity to hyperdissipation
3. Coherent structures (TG, KP) show stronger threshold effects than broadband turbulence

However, we emphasize: these are *diagnostics*, not proofs. The framework monitors regularity-relevant quantities; it does not establish bounds.

7.3 Utility for Numerical Studies

The diagnostic framework provides:

- **Regime classification**: Is the flow cascade- or diffusion-dominated?
- **Early warning**: When should timesteps be reduced or resolution increased?
- **Convergence assessment**: Are diagnostics stable with refinement?
- **Comparative analysis**: Which initial conditions pose greater regularity challenges?

7.4 Relation to Prior Work

Constantin–Fefferman–Majda [2]: Our alignment field $A(x,t)$ is closely related to their geometric blow-up criteria. Heat kernel smoothing provides a viscosity-aware version.

Hou–Li [3]: The observation that stretching can be dynamically depleted connects to our control ratios $\rho_s < 1$.

Gibbon [5]: The three-tier structure (cascade/transitional/diffusion) parallels discussions of regularity criteria hierarchies.

8 Conclusion

We have developed a Tao-inspired diagnostic framework for monitoring vorticity–stretching alignment in 3D Navier–Stokes simulations. The key innovations are:

1. The Re-normalized timescale ratio $\tau_{\text{norm}} = \sqrt{k_{\text{eff}}}/\omega$ provides meaningful regime classification across Reynolds numbers, unlike the classical ratio which saturates.
2. Hyperdissipation threshold effects near $s = 5/4$ are detectable numerically, with coherent flows showing stronger sensitivity.
3. Acceleration-event detection enables predictive early warning for Taylor–Green type flows, with τ_{norm} leading ω by 7–10 timesteps.
4. Systematic validation confirms convergence with resolution and monotonic scaling with Reynolds number.

The framework is implemented atop the BKM Engine, a GPU-accelerated pseudo-spectral solver with continuous regularity monitoring. Code and configurations are available for reproducibility.

This work is computational and exploratory. It provides diagnostic tools, not regularity proofs. We hope it motivates both further numerical investigation at higher Re and resolution, and analytical work connecting these observables to rigorous bounds.

8.1 Future Directions

- $N = 256$ validation to disambiguate physics vs. resolution floor
- Higher Re (> 6400) to approach cascade regime with Taylor–Green
- Extension to other flow configurations (anti-parallel tubes, stratified flows)
- Analytical connection between τ_{norm} bounds and BKM integrals

8.2 Code Availability

Source code available at: `github.com/jdcurry/bkm-engine`

The heat kernel diagnostic module (v5.1) integrates with the unified BKM Engine (v2.0.0).

A Derivation of Re-Normalized Ratio

The classical timescale ratio is

$$\tau_{\text{ratio}} = \frac{\nu\sqrt{k}}{\omega}.$$

For turbulent flows, this is always $\ll 1$ because the critical wavenumber $k_{\text{crit}} = (\omega/\nu)^2$ exceeds resolved scales. Multiplying by $Re = UL/\nu$ (with characteristic velocity U and length L) gives

$$\tau_{\text{norm}} = Re \cdot \tau_{\text{ratio}} = \frac{\sqrt{k} \cdot UL}{\omega \cdot \nu} \cdot \nu = \frac{UL\sqrt{k}}{\omega}.$$

With appropriate non-dimensionalization ($U \sim \omega L$), this reduces to $\tau_{\text{norm}} \sim \sqrt{k}/\omega$, which can span $O(1)$ values.

B Acceleration Event Detection

For monotonically growing vorticity (as in Taylor–Green), peak detection fails. Instead, we detect acceleration phases:

1. Smooth $\omega(t)$ with Gaussian filter ($\sigma = 3$)
2. Compute $\ddot{\omega} = d^2\omega/dt^2$
3. Identify regions where $\ddot{\omega} > 0.1 \cdot \max|\ddot{\omega}|$
4. For each acceleration event, find preceding τ_{norm} minimum
5. Compute lag = (event start time) − (τ_{norm} minimum time)

C Spectral Implementation of k_{eff}

The enstrophy-weighted effective wavenumber:

$$k_{\text{eff}} = \frac{\sum_k |k| \cdot |\hat{\omega}(k)|^2}{\sum_k |\hat{\omega}(k)|^2}$$

This is computed efficiently in Fourier space with a single pass over the vorticity spectrum.

References

[1] Beale, J.T., Kato, T., Majda, A. (1984). Remarks on the breakdown of smooth solutions for the 3D Euler equations. *Comm. Math. Phys.*, 94(1), 61–66.

[2] Constantin, P., Fefferman, C., Majda, A.J. (1996). Geometric constraints on potentially singular solutions for the 3-D Euler equations. *Comm. Partial Differential Equations*, 21(3-4), 559–571.

[3] Hou, T.Y., Li, R. (2006). Dynamic depletion of vortex stretching and non-blowup of the 3-D incompressible Euler equations. *J. Nonlinear Sci.*, 16(6), 639–664.

[4] Tao, T. (2016). Finite time blowup for an averaged three-dimensional Navier–Stokes equation. *J. Amer. Math. Soc.*, 29(3), 601–674.

[5] Gibbon, J.D. (2008). The three-dimensional Euler equations: where do we stand? *Physica D*, 237(14–17), 1894–1904.

[6] Brachet, M.E. (1991). Direct simulation of three-dimensional turbulence in the Taylor–Green vortex. *Fluid Dyn. Res.*, 8(1–4), 1–8.

[7] Kerr, R.M. (1993). Evidence for a singularity of the three-dimensional, incompressible Euler equations. *Phys. Fluids A*, 5(7), 1725–1746.

[8] Donzis, D.A., Yeung, P.K., Sreenivasan, K.R. (2008). Dissipation and enstrophy in isotropic turbulence: resolution effects and scaling in direct numerical simulations. *Phys. Fluids*, 20(4), 045108.